Experimental Mechanics (2021) 61:1081–1092
https://doi.org/10.1007/s11340-021-00748-z

RESEARCH PAPER

Relaxation and Recovery in Hydrogel Friction on Smooth Surfaces

B. Wu[1] · **J. S. Méndez Harper**[1] · **J. C. Burton**[1]

Received: 3 December 2020 / Accepted: 9 June 2021 / Published online: 22 June 2021

Abstract

Background Hydrogels are crosslinked polymer networks that can absorb and retain a large fraction of liquid. Near a critical sliding velocity, hydrogels pressed against smooth surfaces exhibit time-dependent frictional behavior occurring over multiple timescales. The origin of these dynamics is unresolved

Objective Here, we characterize this time-dependent regime and show that it is consistent with two distinct molecular processes: sliding-induced relaxation and quiescent recovery.

Methods Our experiments use a custom pin-on-disk tribometer to examine poly(acrylic acid) hydrogels on smooth poly(methyl methacrylate) surfaces over a variety of sliding conditions, from minutes to hours.

Results We show that at a fixed sliding velocity, the friction coefficient decays exponentially and reaches a steady-state value. The time constant associated with this decay varies exponentially with the sliding velocity, and is sensitive to any precedent frictional shearing of the interface. This process is reversible; upon cessation of sliding, the friction coefficient recovers to its original state. We also show that the initial direction of shear can be imprinted as an observable "memory", and is visible after 24 hrs of repeated frictional shearing.

Conclusions We attribute this behavior to nanoscale extension and relaxation dynamics of the near-surface polymer network, leading to a model of frictional relaxation and recovery with two parallel timescales.

Keywords Hydrogel · Friction · Polymer · Tribology

Introduction

A hydrogel consists of a solvent-saturated, crosslinked polymer network that exhibits unique frictional properties due to its ambiguous nature. When swollen with liquid, osmotic pressure forces from the hydrophillic nature of the polymer network give rise to macroscale elasticity. However, hydrogels can be over 90% liquid by weight, leading to a self-lubricating slippery surface [1–3]. When exposed to a sliding interface, this dichotomy results in non-trivial and time-dependent frictional behavior that is important for numerous applications including biomaterials [4–11], biomechanics [12–15], soft robotics [16–22], and industrial water management [18, 23–29]. The friction coefficient associated with a given interface generally depends on contact geometry [30–35], sliding velocity [36–39], liquid viscosity [40] hydration [41, 42], polymer density [29, 40, 43], and any physicochemical absorption of polymers to the sliding layer [1, 44].

Although hydrogels exhibit interesting bulk rheologies, sliding interfaces expose the near-surface polymers in the network to shear forces that are orders of magnitude larger than those in the bulk. Such strong forces can alter the polymers' entropic configurations and preferentially stretch them in the sliding direction [36, 37, 39–41]. This deformation can result in time-dependent frictional behavior during a single experiment at constant velocity [38–40, 45]. Although the polymers near the interface are generally sparse, forming a crosslinked network with a "mesh size" [46] of order 1-200 nm [29, 40, 47, 48], local entanglements and crosslinking constraints may increase the extension and relaxation rates. In Kim et al. [38, 39, 45] and Cuccia et al. [40] time-dependent frictional behavior was observed over periods of minutes or longer. Furthermore, Cuccia et al. [40] showed that for hydrogels on smooth surfaces, the friction coefficient evolves over multiple timescales which are not directly proportional to liquid viscosity, suggesting that the frictional evolution is not solely due to re-hydration of the interface. The authors suggested that topological polymer entanglements may give rise to a free energy landscape with sufficient complexity to explain the timescales of frictional relaxation and recovery.

✉ J. C. Burton
justin.c.burton@emory.edu

[1] Department of Physics, Emory University, Atlanta, Georgia

Here, we show how the friction between a hydrogel and a smooth surface evolves under a broad set of sliding conditions by rapidly varying the velocity and pre-shearing of the interface. During some experiments, the hydrogel interface is allowed to rest in order to examine the recovery of friction after sliding. For polyacrylic acid (PAA) hydrogels on poly(methyl methacrylate) (PMMA) surfaces, we find that the friction coefficient, μ, only displays time dependent behavior between $v \approx 0.3 - 3$ cm/s, where v is the sliding velocity. For a given sliding velocity in this regime, μ decays exponentially and approaches a steady-state value, independent of the sliding history of the hydrogel. However, the time constant and initial value of the friction do depend on the sliding history. In particular, the time constant decreases exponentially with sliding velocity. Similarly, the recovery of μ is exponential in the waiting time elapsed since the last experiment. We propose a simple, phenomenological model that captures the salient features of this behavior. The model consists of two parallel dynamical processes (relaxation and recovery), with timescales that can vary with the sliding velocity. Finally, and surprisingly, we show how the initial sliding direction can be imprinted as a "memory" into the time evolution of μ, even after 24 hrs of continuous shearing.

Experimental Methods

We performed experiments using the custom pin-on-disk, bi-directional tribometer, illustrated schematically in Fig. 1(a). A similar device was used in Cuccia et al. [40]. A spherical sample – PAA or agarose – of radius $R \approx 7.5$ mm was held stationary to the end of a low-force strain sensor (Strain Measurement Devices S256). This cantilevered spherical sample rested upon a horizontal PMMA substrate fixed to a circular, rotating frame. Using atomic force microscopy, we determined that the root-mean-square roughness of the PMMA to be 3.8 nm over a 1 μm^2 area. The strain sensor measured the tangential force (F_f) on the sphere and was calibrated prior to use. A normal force $F_n = 0.2$ N was applied above the point of contact using a fixed amount of mass under the influence of gravity. The friction coefficient was calculated as $\mu = F_f/F_n$. A macroscopic layer of water over the substrate kept the contact hydrated during the experiment. We varied the thickness of the surrounding water from 1-5 mm and found no difference in the frictional force measurements, so we used a consistent thickness of 3 mm for all experiments reported here. Any bulk drag on the sphere as it moved this layer of fluid would result from velocity gradients over a length scale R, as in Stokes drag. This drag is much smaller than the frictional drag under the contact region, where velocity gradients occur over a length scale d (Fig. 1(c)). All experiments were conducted at 22 ± 2°C.

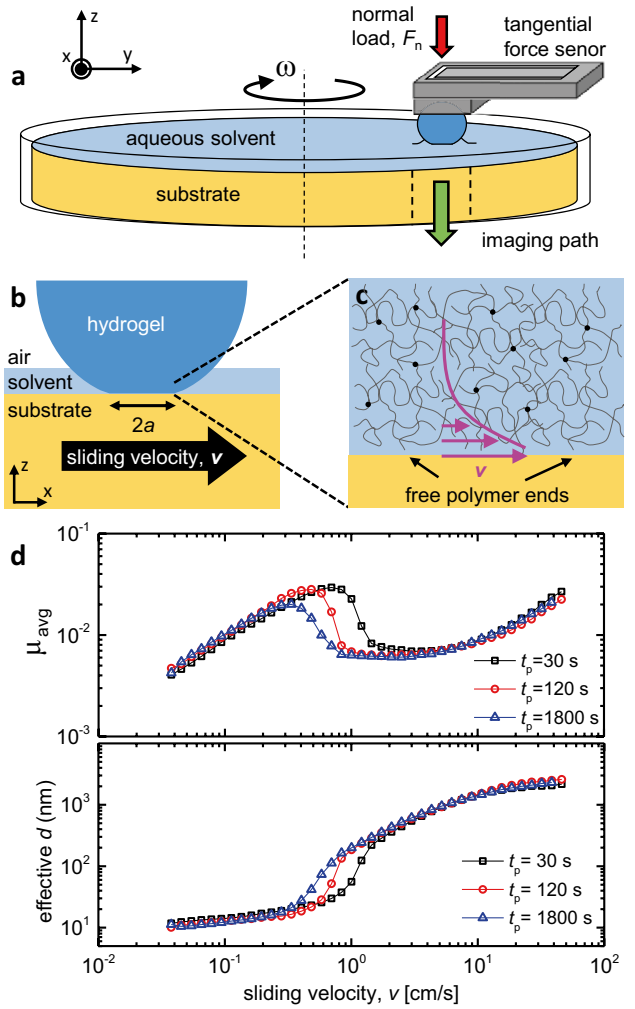

Fig. 1 (**a**) Diagram of the experimental setup showing the spherical sample pressed against the rotating surface. The hydrogel is sheared in the x-direction. (**b**) The characteristic diameter of the circular contact area is $2a$. (**c**) The polymer network adjacent to the surface experiences shear as fluid is dragged through it. (**d**) Plot of μ vs. v for a PAA particle with $F_n = 0.2$ N on an PMMA surface for three different values of the experimental running time, t_p, at each data point. Also shown is the effective decay length of the velocity into the hydrogel, as calculated from (equation (3)) using the viscosity of water (8.9×10^{-4} Pa.s). Error bars are not shown for clarity, but noise from the measurement apparatus is comparable to the point size

The experimental setup was automated using a LabVIEW program. To achieve a broad range of rotational velocities at the point of contact between the spherical sample and the substrate, we drove the substrate with a stepper motor operating in a "microstepping" mode together a set of timing belts. This arrangement allowed us to investigate frictional behaviors at velocities ranging from 0.03 m/s and 60 m/s. The analog voltage at the output of the strain sensor was digitized using a USB data acquisition unit (NI USB-6008) at a rate of 24 kSamples per second. To reduce noise, 12,000 data points were

averaged every 0.5 seconds. Thus, the friction coefficient was effectively measured two times per second. Additionally, we were able to visually assess the point of contact through a milled hole in the structure underlying the spinning substrate.

Individual experiments had durations ranging from 30 s $< t_p <$ 3600 s and the data from each trial was averaged to provide a single value of the friction coefficient μ_{avg}. For some experiments (where indicated), the experiment was paused for 5 s, and then rotated in the opposite direction for the same time t_p in order to average over both directions and calibrate the zero-point of the force sensor. At some velocities, the data displayed an exponential-like decay towards a steady-state value, leading to a large variation in the friction coefficient. We particularly observe these effects within the transition regime when the friction decreased rapidly with sliding velocity. We also observe that this decaying behavior is far more sensitive to changes in speed than changes in direction.

We used two types of hydrogels for our experiments: poly(acrylic acid) (PAA) and agarose. Agarose samples were fabricated in the lab, and the PAA spherical particles were purchased from JRM Chemical (Cleveland, OH). The PAA particles were composed of approximately 70% polyacrylic acid (PAA) and 30% acrylamide monomer, as reported by the manufacturer. Spherical agarose samples were made by mixing agarose (0.5-2.0 g) into 100 ml of distilled water and heating the solution to 60 °C. The solution was then pipetted into a spherical silicone mold and left aside at room temperature for 30 mins. The hydrogel was then immersed in water for at least 2 hrs. All chemicals and solvents used for fabrication were purchased from Millipore Sigma. We measured the ultimate swelling ratio of the gels by immersing them in water and letting them equilibriate. Dry commercial PAA particles, when immersed in water, would swell from an initial radius of ≈ 1 mm to a final radius of ≈ 7.5 mm. Once swollen, the commercial PAA particles consisted of 99.2% water.

Results

Regimes of Frictional Behavior

First it is important to note the distinct regimes of frictional behavior we observe in hydrogels. At low velocities, the hydrogel is pressed firmly against the PMMA surface, making a circular contact area of radius $a \approx 3$ mm (Fig. 1(b)). By varying the normal load and imaging the corresponding contact area using optical microscopy, we confirmed that the hydrogels obeyed a Hertzian relationship [40]. For a sphere pressed against a flat surface, the Hertz theory predicts that

$$a^3 = \frac{3F_n R}{4E^*}, \tag{1}$$

where E^* is the reduced average modulus for the sphere and the substrate:

$$\frac{1}{E^*} = \frac{1-\nu_g^2}{E_g} + \frac{1-\nu_s^2}{E_s}. \tag{2}$$

Here E and ν are the Young's modulus and Poisson's ratio for the gel (g) and substrate (s). The effective modulus for the PAA particles was measured as $E^* \approx 45$ kPa, and for 2% wt agarose it was measured as $E^* \approx 47$ kPa. The contact area was observed from below for some experiments, as was found to be independent of time and velocity [40].

As shown in Fig. 1(c), when the hydrogel is adjacent to the surface, fluid is dragged through the porous polymer network. The characteristic decay length of the velocity is of order the mesh size [40], so that the frictional force is proportional to the viscous shear stress at the interface, as described by Newton's law of viscosity:

$$\mu = \frac{A\eta}{F_n}\frac{v}{d}. \tag{3}$$

Here η is the dynamic viscosity of the solvent, $A = \pi a^2$ is the area of contact, and the velocity gradient has been replaced with v/d, where v is the sliding velocity and d is the effective decay length of the velocity into the hydrogel surface layer (Fig. 1(a)), which is proportional to the pore or "mesh" size of the hydrogel [40]. At low velocities, this leads to a friction coefficient that increases with velocity due to viscous drag (Fig. 1). The friction grows slower than linear with v since d can vary slightly with shear stress [40]. We can solve (equation (3)) for d, and plot the result as a function of velocity, also shown in Fig. 1(d). In the low-velocity regime, the friction coefficient is independent of the amount of time spent measuring it at a given data point (t_p). For the PAA particles used in this study, $d \approx$ 10-30 nm, and for the agarose particles, $d \approx$ 4-8 nm [40]. At high velocities, a bulk fluid layer of thickness ≈ 1 μm develops between the hydrogel and the PMMA surface. In this regime, the friction coefficient is determined by elastohydrodynamic lubrication theory (EHL), and is also independent of t_p. Both the low velocity and high velocity regimes are described in detail in Cuccia et al. [40].

Relaxation of Friction During Sliding

At intermediate velocities (0.3 cm/s $< v <$ 3.0 cm/s), we observe time-dependent dynamics. This can be seen in Fig. 1(d), where the sharp drop in friction and transition to the EHL regime is sensitive to t_p. The variation of μ_{avg} with t_p seen in Fig. 1(d) occurs because the friction decays

exponentially with time during the course of an experiment at a single velocity [40]. At each new data point, μ_{avg} depends on the new velocity, but also on the history of shearing it has experienced. In order to tease apart this history dependence, we performed a series of experiments with a hydrogel particle that has been allowed to "rest" for 2 hrs prior to sliding. Figure 2(a) shows the time evolution of μ after immediately shearing the hydrogel at different velocities for $t_p = 1800$ s. To compare the data, we normalize the data for each experiment by dividing by the maximum μ at $t = 0$ s, denoted as μ_{max}. For low velocities (0.23 cm/s), there is no variation in μ with time. However, at higher velocities, μ decreases and approaches a steady-state value. The rate of decay increases dramatically with velocity.

The data at each sliding velocity is fit remarkably well with a single exponential form,

$$\mu = \Delta\mu \times e^{-\frac{t}{\tau}} + \mu_f, \tag{4}$$

as shown by the solid line in Fig. 2(a). Here, μ_f is the final, steady state friction coefficient, $\Delta\mu = \mu_{max} - \mu_f$ is the change in friction, and τ is the decay time constant. Each of these fitting parameters varied with the sliding velocity, as shown in Fig. 2(b-d). Both $\Delta\mu$ and μ_f reached constant values at high velocities, 0.03 and 0.005, respectively. However, the decay time τ decreased rapidly in this range of sliding velocities, and follows an exponential dependence on v, as shown in Fig. 2(b).

This dependence suggests that the imposed shear may serve as an excitation mechanism to induce relaxation in the polymer network adjacent to the surface. A classical analogy is the α-relaxation time for strong glass formers, which decreases exponentially with inverse temperature [49]. Using (equation (4)), we can also compute the average friction coefficient over the time interval t_p, as was plotted in Fig. 1(d):

$$\mu_{avg} = \mu_f + \Delta\mu\frac{\tau}{t_p}\left(1 - e^{-t_p/\tau}\right). \tag{5}$$

From this it can be seen why μ_{avg} drops so sharply in Fig. 1(d), since τ appears in the exponent, and also decreases exponentially with velocity.

Recovery of Friction During Rest

In addition to exponential relaxation at sliding velocities in the intermediate regime, the friction coefficient also experiences a "recovery" phase upon cessation of sliding. If the shear induced by sliding is able to preferentially align the near-surface polymers and modify the local entanglement

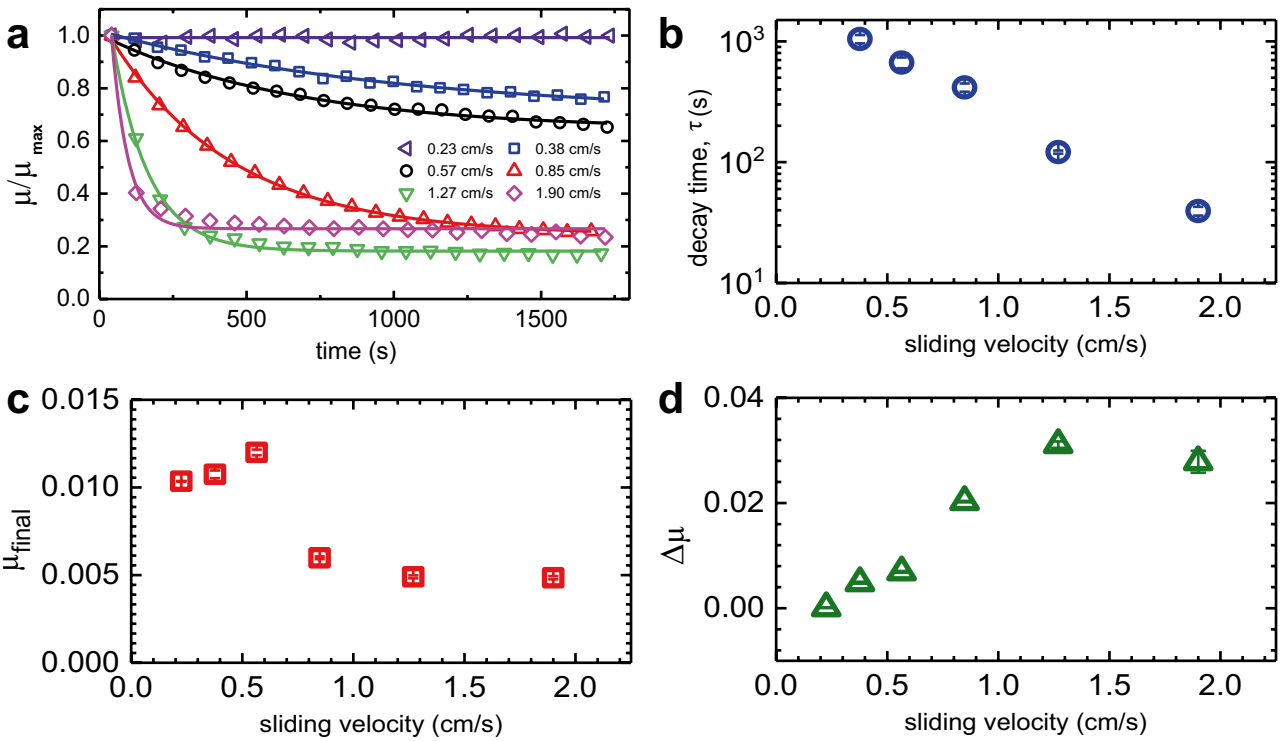

Fig. 2 (**a**) Normalized friction coefficient, μ/μ_{max}, versus time for a spherical PAA hydrogel on a PMMA surface at different sliding velocities. The hydrogel is allowed to "rest" for 2 hrs prior to each experiment. (**b**-**d**) Velocity dependence of parameters obtained from fitting each data set to a single exponential form (equation (4)). Both μ_f and $\Delta\mu$ approach constant values at high velocities, while τ decays exponentially

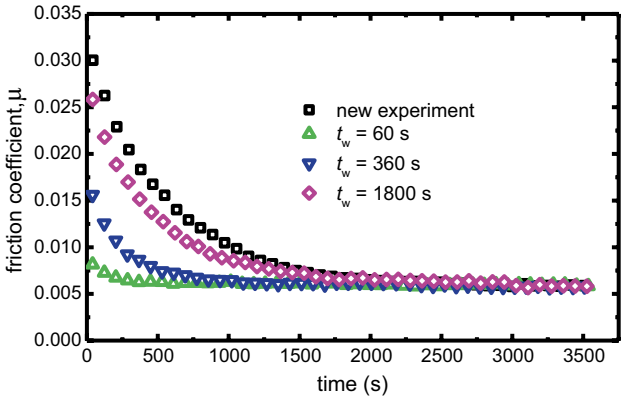

Fig. 3 The friction coefficient μ versus time for a spherical PAA hydrogel being shear at $v = 0.85$ cm/s. "New experiment" corresponds to a hydrogel that has rested for 2 hrs, whereas t_w refers to the elapsed time after shearing that the hydrogel was allowed to wait prior to subsequent shearing

structure of the network, then thermal fluctuations should facilitate a reversible transition to an equilibrium state in the absence of shear. Figure 3 shows a series of experiments where a fresh PAA hydrogel sphere is sheared for 1 hr, and then allowed to rest for a given waiting time t_w. At the end of each experiment, as in Fig. 2(a), the hydrogel is able to reach its final friction coefficient (μ_f). After waiting t_w = 60 s, there is a small amount initial increase in the friction before it rapidly decays again. For larger values of t_w, both μ_{max} and τ increase so that the friction coefficient recovers more and it subsequently takes longer to fully decay again when sliding is initiated. Finally, after waiting 1800 s, the frictional evolution has almost fully recovered to that of a fully-rested hydrogel.

By fitting the time series of μ to the single exponential form (equation (4)) for different values of t_w, we find that μ_{avg}, τ, and $\Delta\mu$ all recover to their initial values after waiting for a sufficiently long time. This is shown in Fig. 4(a-c). The dashed lines show the values associated with experiments from fresh, rested hydrogels. Importantly, even the decay time, τ, seems to depend on the pre-shearing and t_w, changing by roughly a factor of 4 from short to long waiting times. This suggests that during recovery, the polymer network evolves over multiple timescales back to equilibrium. This is reasonable since structural evolution in disordered systems typically contain a variety of timescales due to the ruggedness of the free energy landscape [50]. More specifically, in the case of polymer brushes, the timescale for polymer retraction can be 10^8 or larger than the Rouse time, and can depend on the degree of local entanglement and polymer chain length [51].

All of the data shown in Fig. 4(a-c) are consistent with a generic, single exponential recovery: $y = c_1(1 - e^{-t_w/c_2}) + c_3$, where c_1, c_2, and c_3 are fitting

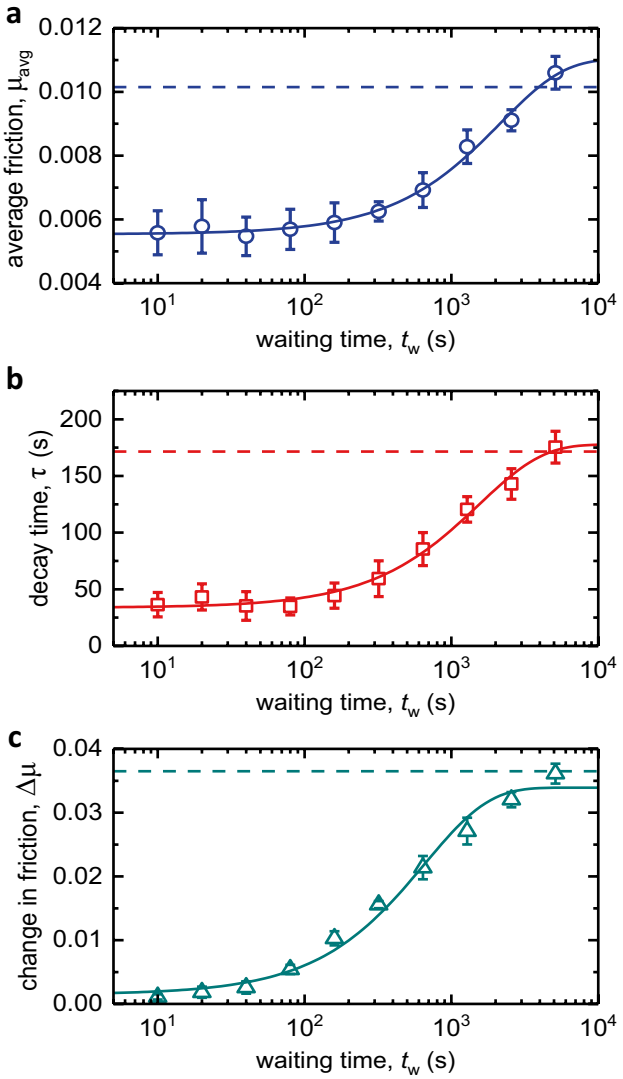

Fig. 4 (**a**) μ_{avg} versus t_w for a PAA hydrogel sphere on PMMA. After initially shearing the hydrogel at $v = 1.27$ cm/s until it has reached a steady state value (μ_f), the hydrogel is allowed to rest for a time t_w. Then data is acquired for $t_p = 600$ s at $v = 1.27$ cm/s for each data point. (**b**) The decay time, τ, versus t_w, obtained from fitting each 600 s time series of μ to (equation (4)). (**c**) The change in friction coefficient, $\Delta\mu$, versus t_w, also obtained from fitting the data to (equation (4)). The solid lines represent exponential fits to the form $y = c_1(1 - e^{-t_w/c_2}) + c_3$, as described in the text. Error bars represent the standard deviations from three separate runs. The dashed lines in each panel represent the average values for a hydrogel which has not experienced prior shearing

parameters. These fits are shown by the solid lines. At the moment, we do not assign physical meaning to these parameters, but the origin of the fitting form will be discussed in Sec. 3.5. We cannot be certain what detailed molecular mechanism accounts for recovery in our experiments without more direct measurements. However, the data necessitates a mechanism that accommodates a range of timescales that are history-dependent. It is unclear if

hydrodynamic models based on lubrication and poroelasticity alone could explain these results. This will be discussed further in Sec. 4.

Asymmetry of Approach to μ_f

The approach to a steady-state friction coefficient, μ_f, depends on the shearing history of the hydrogel, and can be asymmetric. Figure 5 shows the decay in μ from two separate experiments at two different velocities. If the hydrogel is initially rested for 2 hrs before starting an experiment, μ_{avg} starts higher and decreases exponentially to μ_f, as in Fig. 2. However, if the hydrogel is instead sheared at a high velocity, e.g. 3.0 cm/s, for 1800 s, the polymer network is presumably in the "fully sheared" state, far from its equilibrium, rested value. In this regime, μ_f has plateaued with velocity (Fig. 2(c)). By immediately switching back to a lower velocity, the friction coefficient will then *increase* with time, and approach the same value of μ_f.

For both $v = 0.48$ cm/s and $v = 0.58$ cm/s in Fig. 5, the initial value of μ and the decay constant τ is different, but the data for a given velocity tends to the same asymptotic value at long times. This behavior is reminiscent of the Kovacs effect in glassy, disordered materials [52, 53]. The effect is nonlinear in nature since perturbations away from equilibrium follow different relaxation mechanisms. Nevertheless, the fact that μ_f remains the same regardless of the shearing history suggests that the asymptotic sheared state of the system only depends on the sliding velocity.

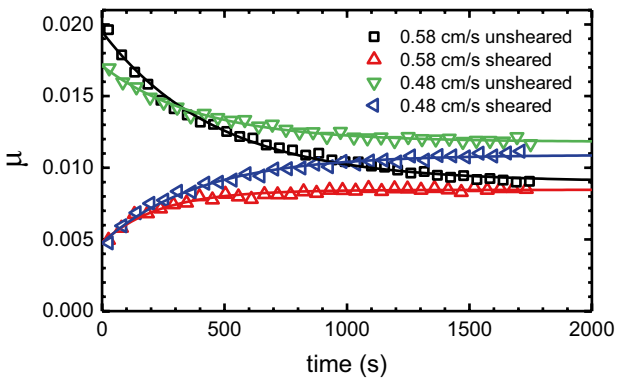

Fig. 5 Time series of the friction coefficient μ for PAA hydrogel on PMMA at with two distinct histories. The black squares and green downward triangles represent frictional relaxation starting from a fully rested gel at 0.58 cm/s and 0.48 cm/s, repsectively. The red upward triangles and blue sideways triangles represent relaxation after the hydrogel has been "fully sheared" at $v = 3.0$ cm/s for 1800 s. The approach to μ_f is asymmetric, with different time constants

Model for Frictional Relaxation and Recovery

The various timescales associated with relaxation and recovery can at first seem complex. However, a simple, phenomenological model with two parallel timescales can capture the qualitative and some of the quantitative features of nearly all data for PAA hydrogel friction in the intermediate regime. We start by introducing a state parameter, γ, which has a range between 0 and 1. This parameterizes the sheared state of the hydrogel network at a given moment. For example, the fully "rested" state with no shearing, $\gamma = 1$, characterizes the state of the polymer network in the low velocity regime, where fluid is dragged through a mostly-isotropic polymer network, and μ is determined by (equation (3)).

In order to be as quantitative as possible, we take into account that μ_{avg} is not perfectly linear in v at low velocities (Fig. 1(d)). Thus, we use a power-law relationship to described μ in this regime:

$$\mu = K_1 v^{\alpha}, \tag{6}$$

where K_1 is a fitting constant and α an exponent close to 1. In our model, we denote the friction coefficient of the hydrogel when $\gamma = 1$ as $\mu_1 = Kv^{\alpha}$. On the other hand, $\gamma = 0$ parameterizes the state where the hydrogel is fully sheared. We define a constant μ_0 to be the lowest friction coefficient that the hydrogel can attain in the time dependent regime. For example, $\mu_f \approx 0.005$ at $v = 1.9$ cm/s in Fig. 2(c). For simplicity, we assume that γ varies linearly between μ_1 and μ_0, or

$$\gamma = \frac{\mu - \mu_0}{\mu_1 - \mu_0}. \tag{7}$$

We now consider the relaxation and recovery processes separately. First, when perturbed by shear, thermal fluctuations will drive the polymers near the surface back to equilibrium ($\gamma = 1$). As shown in Fig. 4(a), this process is well-captured by an exponential fit with a single time constant of order 1000-3000 s. We define this recovery time constant as τ_1 as it refers to recovery to the $\gamma = 1$ state. The evolution of μ is then given by:

$$\frac{d\mu}{dt} = \frac{\mu_1 - \mu}{\tau_1}, \tag{8}$$

We note that the recovery time τ_1 should be independent of sliding velocity, although it may depend on the fluid properties and temperature.

In the absence of recovery processes, the application of a sliding shear will lead to relaxation of μ to the minimum possible value, μ_0. The evolution of μ is then given by

$$\frac{d\mu}{dt} = \frac{\mu_0 - \mu}{\tau_0}, \tag{9}$$

where τ_0 is the time constant associated with relaxation to the $\gamma = 0$ state. As suggested by Fig. 2(b), we assume τ_0 depends on the sliding velocity v:

$$\tau_0 = K_0 e^{-v/v_c}, \tag{10}$$

where the fitting constants K_0 and v_c can be determined by fitting the data in Fig. 2(b).

During an experiment, these two processes are occurring in parallel. The full evolution of $\mu(t)$ is given by combining (equations (8) and (9)):

$$\frac{d\mu}{dt} = \frac{\mu_1 - \mu}{\tau_1} + \frac{\mu_0 - \mu}{\tau_0}, \tag{11}$$

The measured dynamics of μ for a given experiment will depend on its initial shear state γ and the sliding velocity v. Since μ_1 and τ_0 don't explicitly depend on time (only on v), we can solve the equation analytically with the initial condition $\mu(t = 0) = \mu_i$:

$$\mu = (\mu_i - \mu_f)e^{-t/\tau} + \mu_f. \tag{12}$$

The solution is a single exponential decay where

$$\mu_f = \frac{\tau_0\mu_1 + \tau_1\mu_0}{\tau_1 + \tau_0}, \tag{13}$$

$$\tau = \frac{\tau_1\tau_0}{\tau_1 + \tau_0}. \tag{14}$$

With this analytic form, we can recreate much of the data from the experiments. The empirical components of the model are the velocity-dependent forms of μ_1 and τ_0 (equations (6) and (10)). Figure 6 shows analytic predictions which quantitatively capture many of our results. Panels (a-c) correspond to Figs. 1(d), 3, and 5. Panels (d-f) correspond to Fig. 4. By choosing $\mu(t = 0)$ and the sliding velocity v, an analytic time series can be created over a time t_p. This data then serves at the starting condition for the next data point in a simulated experiment shown in Fig. 6.

One of the most important insights from this model is that the effective decay time τ observed during an experiment depends

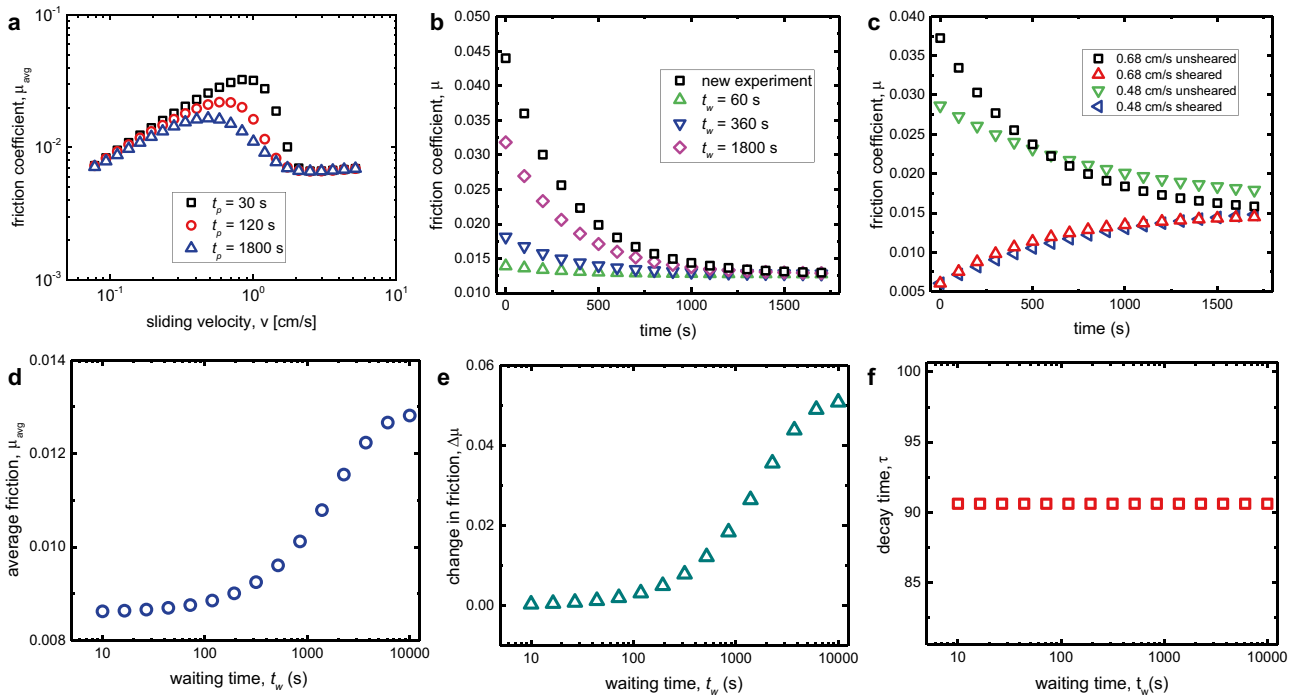

Fig. 6 Results from the analytic model (equation (12)) for different experimental protocols with $\tau_1 = 1910$ s, $K_0 = 8887$ s, $v_c = 0.276$ cm/s, $\mu_0 = 0.006$, $\alpha = 3/4$, and $K_1 = 0.050$ (s/cm)$^{3/4}$. (**a**) Starting from an initial, unsheared state ($\gamma = 1$), μ_{avg} is computed over a time t_p. The value of μ at the end of each period is used as the intial condition for the next sliding velocity. (**b**) Recovery of friction with $v = 0.85$ cm/s. After an initial evolution for 1800 s, the μ evolves with $v = 0$ cm/s for a time t_w. Then sliding proceeds at the same velocity. The value of μ after the recovery period is used as the initial condition for each time series. (**c**) The green downward triangles and black squares show the evolution of μ at the given sliding velocities with no pre-shearing. After evolving μ at $v = 3.0$ cm/s for 1800 s, μ is then allowed to evolve and approach the same steady-state value, demonstrating an asymmetry of approach. (**d-e**) μ_{avg}, $\Delta\mu$, and τ plotted as a function of waiting time t_w. Starting from an unsheared state, μ evolves at $v = 1.27$ cm/s for 600 s, then is allowed to recover for t_w. The value of μ at the end of each times series is used as the initial condition for the next time series

on a parallel combination of two independent time constants (equation (14)). Thus, τ will be smaller than either τ_1 or τ_0. This explains why we observe a variety of timescales for frictional dynamics in our experiments which depend on sliding velocity. Since Fig. 2(b) is technically reporting τ and not τ_0, we convert it to τ using (equation (14)) and then apply (equation (10)) for curve-fitting for all the simulation results reported above.

An important limitation of the model is evident in Fig. 6(f), which shows τ versus t_w. Since τ only depends on sliding velocity in our model and not on t_w, it is constant throughout the modeled experiment. However, as Fig. 4(b) shows, 35 s $\lesssim \tau \lesssim$ 175 s throughout the physical experiment, implying that τ_1 may depend somewhat on the state of the system, γ. This is reasonable since the perturbations from equilibrium can be quite large, and there can simultaneously exist slow and fast timescales due to the large deformation of the polymer network.

Agarose Hydrogels

Although most of our experiments were performed with PAA hydrogel, we also tested agarose hydrogel spheres. In addition to acrylic acid and acrylamide hydrogels, Cuccia et al. [40] reported a similar rise in friction at low velocities for agarose spheres, followed by a sharp drop in friction in the time-dependent regime. However, the dynamics of μ versus t for agarose hydrogels is quite distinct from PAA, and is not exponential. Figure 7(a) shows that μ often starts at rather large values, near 0.4, then drops precipitously with an increasing rate until it reaches values near 0.01 after 100 s of sliding. For these experiments, $\Delta\mu$ can be quite large from the beginning to the end of a time series, more than 10 times the final value μ_f.

Nevertheless, the friction experiences similar recovery times as the PAA hydrogel, and is consistent with an exponential recovery process, as show in Fig. 7(a). Agarose is a physical gel with transient crosslinks, suggesting that its near-surface network structure can be substantially altered due to shear, in contrast to the permanent crosslinks in PAA. We suspect that this may explain the non-exponential behavior and sharp drop in μ in Fig. 7(a), and subsequently the large change in friction upon recovery (Fig. 7(b)). Rather than being perturbed from equilibrium, the local deformation and structural rearrangement is dramatic. However, if the recovery process is controlled by thermal fluctuations proportional to $k_B T$, or possibly by poroelasticity, then the recovery timescales could be similar to PAA. These possibilities will be discussed further in Sec. 4.

Directional Memories in PAA Hydrogels

Finally, we explored the long-time behavior and directional dependence of PAA hydrogel friction. Starting with a fresh

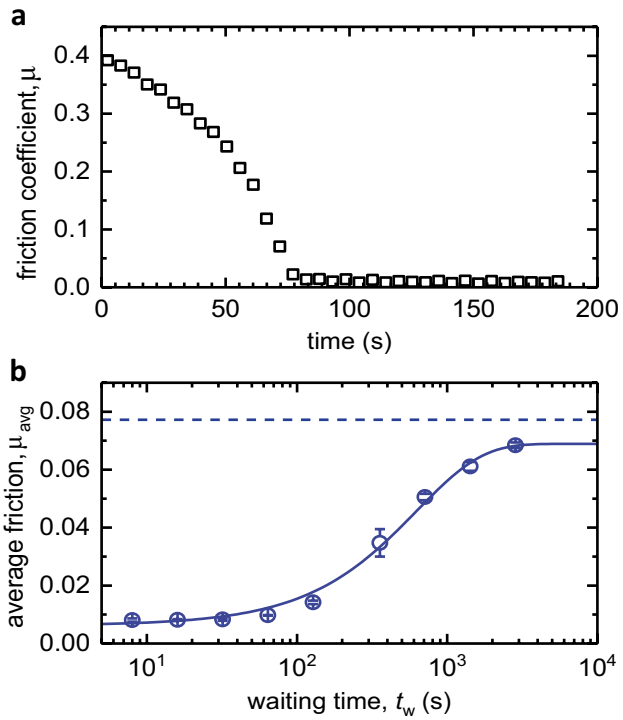

Fig. 7 (**a**) Friction coefficient of a 2% agarose gel on PMMA versus time at $v = 3.94$ cm/s. The gel experiences no prior shearing, and the decay is not exponential. (**b**) The average friction coefficient of agarose gel, μ_{avg}, at $v = 3.94$ cm/s versus waiting time. For each time series, μ_{avg} is computed for $t_p = 600$ s, as in Fig. 4. Error bars represent the standard deviations from three separate runs

hydrogel sphere that did not experience pre-shearing, the frictional force was measured in both the counterclockwise (CCW) and clockwise (CW) direction, each for 1800 s at $v = 0.53$ cm/s. After the initial decay of friction in the CCW direction, we observed relaxation in the CW direction, and recovery in the CCW direction, as shown in Fig. 8. Surprisingly, after 24 hrs, this asymmetry is still present, indicating that the initial direction of shear imprints a "memory" that can be observed at long times.

To confirm that this is not an experimental artifact, we performed separate experiments with fresh hydrogels with different initial shear directions. Figure 8(b-c) shows that μ always experiences recovery when shearing in the initial direction, and relaxation in the opposing direction. However, μ_f was essentially the same in both directions, indicating that the final frictional state of the interface (γ in our model) was independent of direction. We note that this asymmetry cannot be captured by our model in its current form since direction is not explicitly included.

We suspect that this memory is imprinted by some semi-permanent orientational ordering at the hydrogel interface due to the initial sliding. It is unclear if this change would fully recovery given enough rest time, and

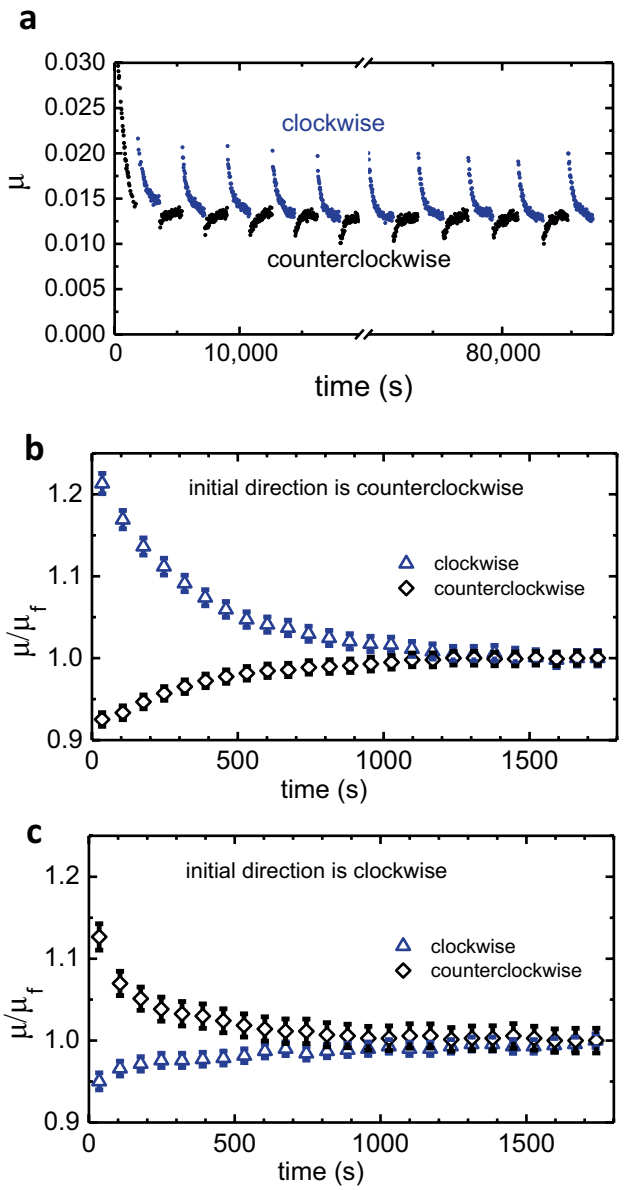

Fig. 8 Directional memories can be imprinted in the frictional evolution of PAA hydrogels. (**a**) Coefficient of friction from a PAA hydrogel sliding on a PMMA disk at $v = 0.53$ cm/s. The inital sliding direction is CCW, and the direction is switched every 1800 s for a total period of 24 hrs. The directional asymmetry in the frictional evolution comes from the choice of the initial sliding direction. Note the break in the abscissa. (**b**-**c**) Averaged data μ/μ_f for CW and CCW directions for $t > 5000$ s shows that recovery always occurs in the initial sliding direction, and relaxation occurs in the opposing direction

warrants further investigation. We did not investigate the directional dependence of agarose hydrogels because the decay time of μ is generally much shorter (Fig. 7), and because agarose is a physical gel that is easily altered in long-duration experiments and may experience wearing of the surface.

Discussion and Summary

The results presented here illustrate unique, time dependent frictional behavior between a hydrogel and a smooth, hard surface. In a range of intermediate sliding velocities, μ experiences a decay toward a new, velocity dependent value with a time constant that is itself velocity dependent. The frictional dynamics are reversible. The frictional state will recover given sufficient resting time, and there is no evidence of permanent wear. This behavior can be modeled quantitatively using two distinct time constants representing shear-induced relaxation and exponential recovery toward equilibrium.

Our semi-quantitative analytic model is similar to other "rate and state" models used recently to describe time-dependent frictional behavior in hydrogels. However, the underlying mechanism leading to time-dependent behavior has not been fully resolved. Similar time-dependent behavior first observed in Kim et al. [39] was modeled using a frictional shear stress that followed two separate power-law behaviors according to a state variable that parameterized the rheological state of the interface [38, 45]. A mechanism involving rehydration of the interface, characterized by a heterogeneous distribution of bulk fluid pockets, was employed to explain the time and velocity dependence. Furthermore, studies examining bovine cartilage at high normal loads showed an exponential decrease in compression and friction vs. time, which was attributed to rehydration [42, 54]. This decrease occurred more rapidly at higher velocities, in analogy with the experiments presented in Fig. 4. However, Meier et al. [55] and Simič et al. [56] showed how the entropic freedom of near-surface polymers alter μ by more than an order of magnitude. They also illustrate an exponential decay of μ whose time constant (while less than 1 minute) decreases with velocity.

As proposed in Cuccia et al. [40], the extremely long relaxation times observed in the experiments, much longer than the Rouse timescale, could be attributed to shear-induced deformation and entanglements of the near-surface polymer layer. This is schematically shown in Fig. 9. The characteristic relaxation time for an isolated polymer blob can be written as $\tau \approx \eta\xi^3/k_BT$, where ξ is the blob or mesh size [43, 46]. The shear rate used in our experiments is of order $\dot{\gamma} \approx v/d \approx v/\xi$, since we are assuming that the characteristic decay length of the velocity into the hydrogel is of order ξ. The Weissenberg number generically describes the threshold for polymers to deform in a shear flow, and is given by $\mathrm{W} = \dot{\gamma}\tau = \eta v\xi^2/k_BT$. For water at room temperature ($\eta \approx 0.0009$ Pa·s), $v = 0.5$-1.0 cm/s, and $\xi \approx 10$-30 nm (Fig. 1(d)), we see that $\mathrm{W} = 0.1$-2.0. This illustrates that the strong shear rates in our experiments, of order 10^5 s^{-1}, are sufficient to initiate deformation of the polymers near the surface.

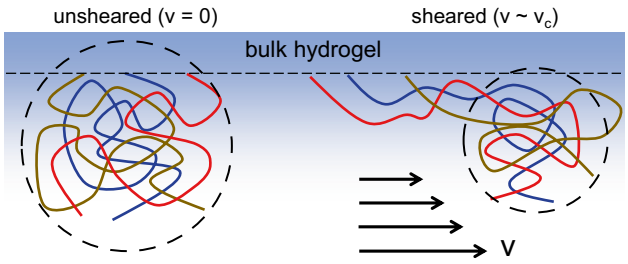

Fig. 9 Potential model for the origin of time-dependent friction observed in our experiments. Near-surface polymers are sparse, yet still remain entangled. Shearing of the polymers by the fluid solvent reduces the available free volume for the topological entanglements, leading to long relaxation times. An increase in the shear rate can activate this process, resulting in an exponential dependence of the relaxation time with velocity. Image adapted from Cuccia et al. [40]

During deformation, the polymer entanglements are pushed to a smaller volume, leading to long relaxation times due to the required cooperative motion for disentanglement. As the shear rate is increased, the free energy barriers to disentanglement are reduced, and thus the relaxation timescale sharply decreases with sliding velocity. Upon the cessation of sliding, thermal fluctuations drive the polymers back to their unsheared state, yet this can also take hundreds to thousands of seconds since it involves the cooperative motion of many polymers near the surface (Fig. 3).

However, long-time, transient behavior could also be expected from fluid flow through the nanoscopic porous polymer network, and thus rehydration of the contact region remains an important consideration. Indeed, a simple estimate using diffusion coefficients for bulk water transport, $D \approx 10^{-9}$ m^2/s [57], and a length scale of $a = 3$ mm, one can arrive at a poroelastic timescale of $\approx 9{,}000$ s. However, in the bulk, moving fluid through the pores requires pressures larger than the osmotic pressure [58, 59], and would lead to contact areas that may vary with time or sliding velocity. According to Hertzian contact theory, the maximum pressure beneath the sliding contact is of order 11 kPa in our experiments, and the osmotic pressure is typically of order 1/2 of the Young's modulus [59, 60]. This would be $E^*/2 \approx 23$ kPa for the PAA and agarose in our experiments, so bulk fluid transport is unlikely. Additionally, as shown in Cuccia et al. [40], the size of the sliding contact does not depend on velocity PAA and agarose gels under similar normal loads.

Nevertheless, the osmotic pressure must approach zero near the surface of the hydrogel. Here the polymer surface layer is "brushy" [56], and the width of this transition region can be 10's of microns thick [57]. Certainly this layer can shrink and swell in response to the addition of water into the contact region when the lubrication pressure of the water can support some of the normal load. Yet the diffusive timescale for transport in and out of this layer is fast (on the order of 1 s) [57], and cannot explain the 30 minute or longer timescales observed in our experiments. It is still possible that rehydration and swelling of this brushy interface is occurring in the transient regime, but we hypothesize that the long timescales and exponential relaxation would still require a restructuring of polymer entanglements near the surface. Very slow, long-time creep has also been observed in compression experiments [58], and was attributed to the diffusion of network heterogeneities rather than poroelasticity based on similar arguments.

Given to preponderance of rehydration as a potential projenitor of time-dependent friction in the literature, it is important to summarize and enumerate why rehydration cannot solely explain our results:

1. The Weissenberg number, $\dot{\gamma}\tau$, is of order unity at the experimentally measured transition velocity, 0.5-1.0 cm/s. This is clear evidence that the polymers near the surface will be affected by the shear flow.
2. The time constant associated with frictional relaxation varies exponentially with velocity (Fig. 4(b), (equation (10)). We are unaware of a rehydration-based explanation for this dependence. A long relaxation time, much longer than expected for an isolated polymer chain, can exist in crowded, entangled polymer brushes [61], and a specific exponential dependence of the relaxation time on shear rate can exist in end-absorbed polymer brushes [62]. For polyacrylamide hydrogels, experiments support this "brushy" approximation near the surface [56, 57].
3. For two separate hydrogels with similar elastic modulii (PAA and agarose), the decay dynamics are different, one exponential (PAA, Fig. 4), and one distinctly non-exponential (agarose, Fig. 7). Agarose is a physical gel and we suspect that permanent alteration to the sliding surface occurs. Nevertheless, poroelastic rehydration is unlikely to explain this strong asymmetry between the gels.
4. The recovery (increase) in μ observed in our experiments after shearing, i.e. Fig. 5, shows that the hydrogel surface has been structurally altered after shearing at higher velocities. The friction is more than a factor of 2 *lower* than it would be if a fresh, fully-swollen gel had been tested. If this were due to rehydration, the lubrication pressure (≈ 7 kPa) would need to significantly "overswell" the gel surface layer well beyond its equilibrium, unloaded value, and require nearly 1800 s to recover.
5. The directional memories observed for 24 hrs simply cannot be explained by a model that only considers swelling and rehydration from flows perpendicular to the hydrogel's surface.

The hydrogel interface remains a subject of active research due to it's complex nature. Our results for hydrogels on smooth surfaces represent a significant advance in our understanding of the polymer network's response to high shear rates, yet there remains many unanswered questions. Ultimately, experiments involving a molecular probe of the surface dynamics may resolve many of these issues surrounding the importance of local polymer physics versus poroelasticity in determining the transient frictional response.

Acknowledgements The authors would like to acknowledge support from NSF DMR Grant No. 14550869, and also from the Emory SURE summer program for undergraduate research.

Declarations

Conflicts of Interest The authors declare that they have no conflict of interest.

References

1. Gong JP (2006) Friction and lubrication of hydrogels—its richness and complexity. Soft Matter 2:544–552. https://doi.org/10.1039/b603209p
2. Bonyadi SZ, Hasan MM, Kim J, Mahmood S, Schulze KD, Dunn AC (2020) Review: Friction and lubrication with high water content crosslinked hydrogels. Tribol Lett 68:1–15. https://doi.org/10.1007/s11249-020-01352-3
3. Shoaib T, Espinosa-Marzal RM (2020) Advances in understanding hydrogel lubrication. Colloids Interfaces 4. https://doi.org/10.3390/colloids4040054
4. Moore AC, DeLucca JF, Elliott DM, Burris DL (2016) Quantifying cartilage contact modulus, tension modulus, and permeability with hertzian biphasic creep. J Tribol 138. https://doi.org/10.1115/1.4032917
5. Moore A, Burris D (2015) Tribological and material properties for cartilage of and throughout the bovine stifle: support for the altered joint kinematics hypothesis of osteoarthritis. Osteoarthr Cartilag 23:161–169. https://doi.org/10.1016/j.joca.2014.09.021
6. Moore A, Burris D (2014) An analytical model to predict interstitial lubrication of cartilage in migrating contact areas. J Biomech 47:148–153. https://doi.org/10.1016/j.jbiomech.2013.09.020
7. Rennie AC, Dickrell PL, Sawyer WG (2005) Friction coefficient of soft contact lenses: measurements and modeling. Tribol Lett 18:499–504. https://doi.org/10.1007/s11249-005-3610-0
8. Lee KY, Mooney DJ (2001) Hydrogels for tissue engineering. Chem Rev 101:1869–1880. https://doi.org/10.1021/cr000108x
9. Dong L, Agarwal AK, Beebe DJ, Jiang H (2006) Adaptive liquid microlenses activated by stimuli-responsive hydrogels. Nature 442:551–554. https://doi.org/10.1038/nature05024
10. Hamidi M, Azadi A, Rafiei P (2008) Hydrogel nanoparticles in drug delivery. Adv Drug Delivery Rev 60:1638–1649. https://doi.org/10.1016/j.addr.2008.08.002
11. Larson C, Peele B, Li S, Robinson S, Totaro M, Beccai L, Mazzolai B, Shepherd R (2016) Highly stretchable electroluminescent skin for optical signaling and tactile sensing. Science 351:1071–1074. https://doi.org/10.1126/science.aac5082
12. Greene GW, Banquy X, Lee DW, Lowrey DD, Yu J, Israelachvili JN (2011) Adaptive mechanically controlled lubrication mechanism found in articular joints. Proc Natl Acad Sci USA 108:5255–5259. https://doi.org/10.1073/pnas.1101002108
13. Lieleg O, Ribbeck K (2011) Biological hydrogels as selective diffusion barriers. Trends Cell Biol 21:543–551. https://doi.org/10.1016/j.tcb.2011.06.002
14. Kisiday J, Jin M, Kurz B, Hung H, Semino C, Zhang S, Grodzinsky AJ (2002) Self-assembling peptide hydrogel fosters chondrocyte extracellular matrix production and cell division: Implications for cartilage tissue repair. Proc Natl Acad Sci USA 99:9996–10001. https://doi.org/10.1073/pnas.142309999
15. Barth H, Crafoord S, Andréasson S, Ghosh F (2016) A cross-linked hyaluronic acid hydrogel (healaflow®) as a novel vitreous substitute. Graefes Arch Clin Exp Ophthalmol 254:697–703. https://doi.org/10.1007/s00417-015-3256-z
16. Beebe DJ, Moore JS, Bauer JM, Yu Q, Liu RH, Devadoss C, Jo BH (2000) Functional hydrogel structures for autonomous flow control inside microfluidic channels. Nature 404:588–590. https://doi.org/10.1038/35007047
17. Sidorenko A, Krupenkin T, Taylor A, Fratzl P, Aizenberg J (2007) Reversible switching of hydrogel-actuated nanostructures into complex micropatterns. Science 315:487–490. https://doi.org/10.1126/science.1135516
18. Sun JY, Zhao X, Illeperuma WRK, Chaudhuri O, Oh KH, Mooney DJ, Vlassak JJ, Suo Z (2012) Highly stretchable and tough hydrogels. Nature 489:133–136. https://doi.org/10.1038/nature11409
19. Bauer S, Bauer-Gogonea S, Graz I, Kaltenbrunner M, Keplinger C, Schwödiauer R (2013) 25th anniversary article: A soft future: From robots and sensor skin to energy harvesters. Adv Mater 26:149–162. https://doi.org/10.1002/adma.201303349
20. Keplinger C, Sun J-Y, Foo CC, Rothemund P, Whitesides GM, Suo Z (2013) Stretchable, transparent, ionic conductors. Science 341:984–987. https://doi.org/10.1126/science.1240228
21. Kim YS, Liu M, Ishida Y, Ebina Y, Osada M, Sasaki T, Hikima T, Takata M, Aida T (2015) Thermoresponsive actuation enabled by permittivity switching in an electrostatically anisotropic hydrogel. Nat Mater 14:1002–1007. https://doi.org/10.1038/nmat4363
22. Yuk H, Lin S, Ma C, Takaffoli M, Fang NX, Zhao X (2017) Hydraulic hydrogel actuators and robots optically and sonically camouflaged in water. Nat Commun 8:14230. https://doi.org/10.1038/ncomms14230
23. Zhu D, Wei L, Wang B, Feng Y (2014) Aqueous hybrids of silica nanoparticles and hydrophobically associating hydrolyzed polyacrylamide used for eor in high-temperature and high-salinity reservoirs. Energies 7:3858–3871. https://doi.org/10.3390/en7063858
24. Abidin AZ, Puspasari T, Nugroho WA (2012) Polymers for enhanced oil recovery technology. Procedia Chem 4:11–16. https://doi.org/10.1016/j.proche.2012.06.002
25. Chen L, Zhang G, Ge J, Jiang P, Zhu X, Ran Y, Han S (2015) Ultrastable hydrogel for enhanced oil recovery based on double-groups cross-linking. Energy Fuels 29:7196–7203. https://doi.org/10.1021/acs.energyfuels.5b02124
26. Tongwa P, Nygaard R, Bai B (2012) Evaluation of a nanocomposite hydrogel for water shut-off in enhanced oil recovery applications: Design, synthesis, and characterization. J Appl Polymer Sci 128:787–794. https://doi.org/10.1002/app.38258
27. Guilherme MR, Aouada FA, Fajardo AR, Martins AF, Paulino AT, Davi MF, Rubira AF, Muniz EC (2015) Superabsorbent hydrogels based on polysaccharides for application in agriculture as soil conditioner and nutrient carrier: A review. Eur Polym J 72:365–385. https://doi.org/10.1016/j.eurpolymj.2015.04.017
28. Rudzinski WE, Dave AM, Vaishnav UH, Kumbar SG, Kulkarni AR, Aminabhavi TM (2002) Hydrogels as controlled release devices in agriculture. Des Monomers Polym 5:39–65. https://doi.org/10.1163/156855502760151580

29. Kim S, Iyer G, Nadarajah A, Frantz JM, Spongberg AL (2010) Polyacrylamide hydrogel properties for horticultural applications. Inte J Polymer Anal Charact 15:307–318. https://doi.org/10.1080/1023666X.2010.493271
30. Saintyves B, Jules T, Salez T, Mahadevan L (2016) Self-sustained lift and low friction via soft lubrication. Proc Natl Acad Sci USA 113:5847–5849. https://doi.org/10.1073/pnas.1525462113
31. Pandey A, Karpitschka S, Venner CH, Snoeijer JH (2016) Lubrication of soft viscoelastic solids. J Fluid Mech 799:433–447. https://doi.org/10.1017/jfm.2016.375
32. Urzay J, Smith SGL, Glover BJ (2007) The elastohydrodynamic force on a sphere near a soft wall. Phys Fluids 19. https://doi.org/10.1063/1.2799148
33. Skotheim JM, Mahadevan L (2005) Soft lubrication: The elastohydrodynamics of nonconforming and conforming contacts. Phys Fluids 17. https://doi.org/10.1063/1.1985467
34. Skotheim JM, Mahadevan L (2004) Soft lubrication. Phys Rev Lett 92. https://doi.org/10.1103/physrevlett.92.245509
35. Yashima S, Takase N, Kurokawa T, Gong JP (2014) Friction of hydrogels with controlled surface roughness on solid flat substrates. Soft Matter 10:3192–3199. https://doi.org/10.1039/c3sm52883a
36. Pitenis AA, Urueña JM, Schulze KD, Nixon RM, Dunn AC, Krick BA, Sawyer WG, Angelini TE (2014) Polymer fluctuation lubrication in hydrogel gemini interfaces. Soft Matter 10:8955–8962. https://doi.org/10.1039/c4sm01728e
37. Dunn AC, Pitenis AA, Na JMU, Schulze KD, Angelini TE, Sawyer WG (2015) Kinetics of aqueous lubrication in the hydrophilic hydrogel gemini interface. Proc Inst Mech Eng H 229:889–894. https://doi.org/10.1177/0954411915612819
38. Kim J, Dunn AC (2018) Thixotropic mechanics in soft hydrated sliding interfaces. Tribology Letters 66. https://doi.org/10.1007/s11249-018-1056-4
39. Kim J, Dunn AC (2016) Soft hydrated sliding interfaces as complex fluids. Soft Matter 12:6536–6546. https://doi.org/10.1039/c6sm00623j
40. Cuccia NL, Pothineni S, Wu B, Harper JM, Burton JC (2020) Pore-size dependence and slow relaxation of hydrogel friction on smooth surfaces. Proc Natl Aca Sci USA 117:11247–11256. https://doi.org/10.1073/pnas.1922364117
41. Reale ER, Dunn AC (2017) Poroelasticity-driven lubrication in hydrogel interfaces. Soft Matter 13:428. https://doi.org/10.1039/c6sm02111e
42. Moore A, Burris D (2017) Tribological rehydration of cartilage and its potential role in preserving joint health. Osteoarthr Cartilage 25:99–107. https://doi.org/10.1016/j.joca.2016.09.018
43. Urueña JM, Pitenis AA, Nixon RM, Schulze KD, Angelini TE, Sawyer WG (2015) Mesh size control of polymer fluctuation lubrication in gemini hydrogels. Biotribology 1–2:24–29. https://doi.org/10.1016/j.biotri.2015.03.001
44. Gong J, Osada Y (1998) Gel friction: A model based on surface repulsion and adsorption. J Chem Phys 109:8062–8068. https://doi.org/10.1063/1.477453
45. Kim J, Dunn AC (2020) Generalized rate-and-state model linking rheology and soft matter tribology. Extreme Mech Lett 41. https://doi.org/10.1016/j.eml.2020.101013
46. de Gennes PG (1979) Scaling Concepts in Polymer Physics. Cornell University Press
47. Scherer GW (1994) Hydraulic radius and mesh size of gels. J Sol-Gel Sci Technol 1:285–291. https://doi.org/10.1007/BF00486171
48. Tsuji Y, Li X, Shibayama M (2018) Evaluation of mesh size in model polymer networks consisting of tetra-arm and linear poly(ethylene glycol)s. Gels 4:50. https://doi.org/10.3390/gels4020050
49. Angell CA (1995) The old problems of glass and the glass transition, and the many new twists. Proc Natl Acad Sci USA 92:6675–6682. https://doi.org/10.1073/pnas.92.15.6675
50. Berthier L, Biroli G (2011) Theoretical perspective on the glass transition and amorphous materials. Rev Mod Phys 83:587. https://doi.org/10.1103/RevModPhys.83.587
51. Lang M, Werner M, Dockhorn R, Kreer T (2016) Arm retraction dynamics in dense polymer brushes. Macromolecules 49:5190–5201. https://doi.org/10.1021/acs.macromol.6b00761
52. Kovacs AJ (1963) Transition vitreuse dans les polymères amorphes. etude phénoménologique. Fortschr. Hochpolym.-Forsch 3:394–507. https://doi.org/10.1007/BFb0050366
53. Banik S, McKenna GB (2018) Isochoric structural recovery in molecular glasses and its analog in colloidal glasses. Phys Rev E 97. https://doi.org/10.1103/PhysRevE.97.062601
54. Putignano C, Burris D, Moore A, Dini D (2021) Cartilage rehydration: The sliding-induced hydrodynamic triggering mechanism. Acta Biomaterialia 125:90–99. https://doi.org/10.1016/j.actbio.2021.02.040
55. Meier YA, Zhang K, Spencer ND, Simic R (2019) Linking friction and surface properties of hydrogels molded against materials of different surface energies. Langmuir 35:15805–15812. https://doi.org/10.1021/acs.langmuir.9b01636
56. Simic R, Yetkin M, Zhang K, Spencer ND (2020) Importance of hydration and surface structure for friction of acrylamide hydrogels. Tribol Lett 68:64. https://doi.org/10.1007/s11249-020-01304-x
57. Johnson CL, Dunn AC (2021) Tribological characterization of gradient-density polyacrylamide hydrogel surfaces. Exp, Mech. https://doi.org/10.1007/s11340-021-00704-x
58. Schulze KD, Hart SM, Marshall SL, O'Bryan CS, NA JMU, Pitenis AA, Sawyer WG, Angelini TE (2017) Polymer osmotic pressure in hydrogel contact mechanics. Biotribology 11:3–7. https://doi.org/10.1016/j.biotri.2017.03.004
59. Bhattacharyya A, O'Bryan C, Ni Y, Morley CD, Taylor CR, Angelini TE (2020) Hydrogel compression and polymer osmotic pressure. Biotribology 22. https://doi.org/10.1016/j.biotri.2020.100125
60. Schulze KD, Bennett AI, Marshall S, Rowe KG, Dunn AC (2016) Real area of contact in a soft transparent interface by particle exclusion microscopy. J Tribol 138. https://doi.org/10.1115/1.4032822
61. Ruths M, Johannsmann D, Rühe J, Knoll W (2000) Repulsive forces and relaxation on compression of entangled, polydisperse polystyrene brushes. Macromolecules 33:3860–3870. https://doi.org/10.1021/ma9920994
62. Aubouy M, Harden JL, Cates ME (1996) Shear-induced deformation and desorption of grafted polymer layers. J Phys II France 6:969–984. https://doi.org/10.1051/jp2:1996111